IEEE Journal of Microwaves

Received 8 July 2022; revised 11 August 2022; accepted 15 August 2022. Date of publication 9 September 2022; date of current version 6 January 2023.

Digital Object Identifier 10.1109/JMW.2022.3199989

Millimeter-Wave Induced Heating of Cutaneous Nerves and Capillaries

ZAIN HAIDER [1], JULIEN MODOLO [2] (Member, IEEE), MICAELA LIBERTI [3] (Member, IEEE), FRANCESCA APOLLONIO [3] (Member, IEEE), AND MAXIM ZHADOBOV [1] (Senior Member, IEEE)

(Regular Paper)

[1]Centre National de la Recherche Scientifique, (Institut d'Électronique et des Technologies du numéRique), University of Rennes, F-35000 Rennes, France
[2]LTSI, University of Rennes, F-35000 Rennes, France
[3]Department of Information Engineering and Electronics and Telecommunications (DIET), Sapienza University of Rome, 00185 Rome, Italy

CORRESPONDING AUTHOR: Zain Haider (e-mail: zainh1012@gmail.com).

This work was supported in part by the French National Research Program for Environmental and Occupational Health of ANSES under Grant 2018/2 RF/07 through the NEAR 5G Project, in part by the French government support granted to the CominLabs excellence laboratory and managed by the French National Research Agency through the Investing for the Future Program under Grant ANR-10-LABX-07-01, in part by the European Union through the European Regional Development Fund (ERDF), and in part by the French Region of Brittany, Ministry of Higher Education and Research, Rennes Métropole and Conseil Départemental 35, through the CPER Project SOPHIE / STIC & Ondes.
This work did not involve human subjects or animals in its research.

ABSTRACT In this study, we quantify microscale heating at the level of cutaneous nerves and capillaries due to continuous and pulsed plane-wave exposure at 60 GHz. The thermal properties of the nerves and capillaries were derived using mixture equations based on their water content. The electromagnetic problem was solved in conjunction with Pennes bioheat equation and Arrhenius equation using finite element method to evaluate the spatial and temporal evolution of temperature along with thermal damage within cutaneous nerves and capillaries. Although, the maximum power density within the nerve (41.6 kW/m^3) and capillary (20 kW/m^3) was 37.3% and 30.2% higher than surrounding skin for a continuous exposure at 10 W/m^2, the peak temperature elevation (ΔT) within the nerve (93.3 n°C) and capillary (90.7 n°C) occurred after 5 μs and 10 μs of exposure and was 19.2% and 17.7% higher than surrounding skin, respectively. The nerve and capillary attained thermal equilibrium with skin after roughly 10 ms. The maximal ΔT within the nerve (0.5 °C) and capillary (0.25 °C) due to nano- and micro-second 60 GHz pulses with highest fluence (0.48 kJ/m^2) permitted under ICNIRP guidelines was 34% and 24% higher than in the surrounding skin. Ten 3 μs 60 GHz pulses (power density = 13.4 GW/m^2) separated by 10 s of cooling period were used to demonstrate the possibility of selective thermal ablation of cutaneous nerves [damage index (Ω)=1.1)] without damaging skin (Ω = 0.15). The results provide valuable insights into local millimeter-wave induced heating within various skin substructures.

INDEX TERMS Finite element method, human skin, millimeter waves, MTT 70th Anniversary Special Issue, thermal dosimetry.

I. INTRODUCTION

The deployment of millimeter-wave (mmWave) based communication networks has been accelerating due to relentless demand for high-data-rate (multi-GB/s) links [1]. The mmWave enabled fifth generation (5 G) cellular networks are envisioned to provide ultra-low latency (<1 ms), ubiquitous connectivity and massive system capacity (100x >4 G) [2], [3]. Besides 5 G, applications of mmWaves also include high-speed indoor wireless communications (WiGig at 60 GHz), automotive radars (77 GHz), security systems and medical imaging [4], [5]. The wide spread use of mmWave technologies will induce into the environmental spectrum new types of radiations to which humans have never been exposed during evolution.

In contrast to centimeter and decimeter waves, nearly all of the incident power density (*IPD*) of mmWaves is absorbed within the first millimeter at the human body surface [6]. It is well known that mmWave energy is transformed into

heat within the superficial tissues (skin and eyes) due to the rotation of polar water molecules. In order to safeguard against thermal effects of mmWave exposure, the International Commission on Non-Ionizing Radiation Protection (ICNIRP) recommends that the temperature rise within skin and eyes do not exceed 5°C above their normal baseline temperature (33–36 °C) [7]. Similar values are also mentioned in IEEE C95.1 standard [41].

To quantify mmWave-induced heating inside skin, the Pennes bioheat equation is solved analytically and numerically [8], [9]. In most dosimetry studies, the analytical solution of the bioheat equation is obtained by assuming skin as a homogeneous planar medium [6]. Heating of various tissue layers is more accurately described by multilayer models, which take into account underlying fat and muscle tissue. It was highlighted by Kanezaki et al. [10] that compared to a homogeneous model, the surface temperature elevation in a multilayer model can be up to 2.8 times higher because of the insulating nature of the fat layer. Similarly, the Monte Carlo analysis performed by Sasaki et al. showed that steady state temperature elevation in skin is more strongly dependent on thickness of the subcutaneous layers compared to the uncertainties in their electromagnetic properties [11]. Moreover, the surface temperature elevation within the multilayer model incorporating various cutaneous layers (stratum corneum and epidermis) was also found to be higher (factor of three) than in a homogeneous model [12].

The role of local vasodilation in reducing mmWave induced temperature elevation within skin was indicated by the enlightening work of Alekseev et al. [13]. A similar effort by Ziskin et al. showed that cooling effect of dermal blood perfusion increases with thickness of dermis [6]. Further insights into mmWave-induced skin heating were provided by a simplified surface heating model proposed by Foster et al. [14]. The surface heating model was used by Foster et al. to show that pulsed mmWave exposure can lead to higher temperature elevation within skin compared to continuous mmWave exposure with similar fluence [15]. The significance of forced air convection to selectively focus mmWave induced heating within cutaneous layers was revealed in [16]. Recently, it was reported that skin temperature elevation due to mmWave exposure increases (13% at 60 GHz) with age (5–70 years) [17]. The presence of textiles can also enhance (46% at 60 GHz) mmWave induced skin heating compared to the bare skin [18]. Lastly, skin equivalent homogeneous phantoms have also been proposed for estimating mmWave induced skin surface heating [19], [20].

The thermal dosimetry at mmWaves has also been performed by using anthropomorphic computational models [21]. Finite difference method has emerged as the method of choice for solving bioheat equation numerically in these anatomical models [22]. The skin tissue is assumed to be homogeneous in these body models. A comprehensive review on mmWave computational dosimetry studies spanning three decades (1990–2020) was recently published by Hirata et al. [9].

Human skin has an inhomogeneous nature. It contains nerves, sweat glands, hair, arrector pili muscle, sebaceous glands, Meissner corpuscles, Pacinian corpuscles, blood and lymphatic vessels. A priori knowledge of temperature distribution within the skin appendages is essential for capturing any local or systemic thermal effects of mmWaves. The first attempt to evaluate the local temperature elevation within skin due to the presence of sweat ducts was made by Shafirstein et al. [23]. The mmWave energy was selectively absorbed by the sweat ducts due to their higher water content (≈99%), and the temperature maxima within the skin shifted from dermis to epidermis. A similar study was performed by Foster et al. to demonstrate that heating of microscale sweat ducts is biologically insignificant (65 μK) under realistic exposure scenarios (10 W/m^2) [24]. None of the previous studies quantified the temperature elevation within cutaneous nerves and capillaries due to mmWave exposure. We recently demonstrated that compared to the surrounding skin, the cutaneous nerves (37.9%) and capillaries (30.6%) preferentially absorb mmWave power [25].

In this computational study, for the first time, we quantify the microscale heating at the level of cutaneous nerves and capillaries within human skin at 60 GHz.

II. MATERIALS AND METHODS

A. GEOMETRIC MODEL

The skin was modeled with three planar layers: stratum corneum, epidermis and dermis. The thicknesses of stratum corneum (8.08–13.66 μm), epidermis (31.2–189.2 μm) and dermis (0.46–1.9 mm) were 11 μm, 120 μm and 1 mm respectively [25]. The lateral dimensions (x × y) of the skin layers were 25 μm × 61.5 μm (nerve) and 50 μm × 100 μm (capillary) (Fig. 1).

1) CUTANEOUS NERVES

The Aδ fiber was modeled with a curved cylinder embedded in epidermis. The diameter (1–6 μm) and length of Aδ fiber were 3 μm and 26.5 μm, respectively. Although, the Aδ fiber was located at a depth of 16 μm from the skin surface, the nerve fibers are present within all vital layers of epidermis and can be as close as 0.4 μm to the stratum corneum [25]. The nerve fibers move through epidermis both laterally and upwards towards the skin surface in an irregular course and end in small enlargements [43]–[44]. The nerve terminations were not modeled in this study. The truncated model of Aδ fiber shown in Fig. 1(b) was used in order to reduce computational time.

2) CUTANEOUS CAPILLARIES

The electron microscopic studies have shown that capillary loop within dermis exhibits a hair-pin structure [45]–[47]. It was represented with a meandered cylinder as shown in Fig. 1(d). The diameter (3.5–6 μm), length (23.3–270 μm) and width (32–46.1 μm) of the capillary loop were 4.75 μm, 42 μm and 45 μm, respectively [25]. The capillary loop was positioned at a depth of 150 μm from the skin surface [26].

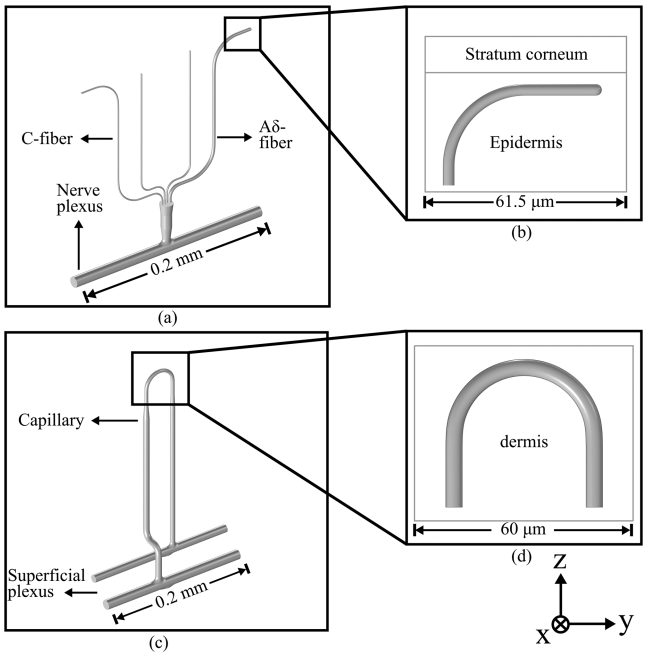

FIGURE 1. Geometric model: (a) cutaneous nerves; (b) terminal section of Aδ fiber; (c) cutaneous blood vessels; (d) capillary loop.

TABLE 1. Relative Permittivity at 60 GHz

Compartment	Complex Permittivity
Stratum corneum	3.5-0.51j
Epidermis and Dermis	8.17-11.27j
Blood	12.3-16.4j
Axoplasm	13.04-18.46j

B. ELECTROMAGNETIC MODEL

The temperature elevation within the cutaneous nerve and capillary due to continuous and pulsed plane wave exposure at 60 GHz was computed in two steps using the finite element method in COMSOL Multiphysics. First, electromagnetic wave equation (1) subject to following boundary conditions was solved using RF module to determine electric field ($\boldsymbol{E}$) within skin.

$$\nabla \times \mu^{-1}(\nabla \times \boldsymbol{E}) - k_0^2 \epsilon(\omega)\boldsymbol{E} = 0 \tag{1}$$

where k_0 is the wave number in free space, ω is the angular frequency; $\epsilon(\omega)$ is the complex relative permittivity @ 60 GHz, and μ is the permeability. The electromagnetic properties of the stratum corneum, epidermis, dermis, nerve and capillary were taken from [25] (Table 1). The equation (1) was solved with perfect electric conductor boundary condition in the ±y directions and perfect magnetic conductor boundary condition in the ±x directions in order to establish the TEM mode.

The mmWave source was modeled as a port. Four exposure scenarios were considered: i) continuous plane wave exposure at 10 W/m^2; ii) pulsed plane wave exposure by one, three and five 2 μs-pulses (50% duty cycle) with *IPD* of 480 MW/m^2, 160 MW/m^2 and 96 MW/m^2 respectively; iii) pulsed plane wave exposure by one, three and five 2 ns-pulses (50% duty cycle) with *IPD* of 480 GW/m^2, 160 GW/m^2 and 96 GW/m^2 respectively; iv) pulsed plane wave exposure by ten 3 μs-pulses (*IPD* = 13.4 GW/m^2) separated by a cooling period of 10 s. Events interface (COMSOL) was used to implement pulsed exposure. The high intensity pulses used in the second and third exposure scenarios are within the limits prescribed by ICNIRP on pulse fluence (0.48 kJ/m^2 at 60 GHz). Higher power was required for the fourth exposure scenario in order to perform selective ablation of cutaneous nerves. Note that the aforementioned extreme worst-case exposure scenarios were selected for illustrating the capability of mmWaves and are not representative of exposure from commonly used mmWave communication devices.

A second order scattering boundary condition was used at the base of dermis to absorb the outgoing wave. Lastly, the power deposition per unit volume (power loss density [*PLD*] in W/m^3) within the skin was calculated from the electric field as follows:

$$PLD = \frac{1}{2}(\sigma_s + \omega\epsilon'')\,|\boldsymbol{E}|^2 \tag{2}$$

where σ_s is the static conductivity and ϵ'' is the imaginary part of complex permittivity.

C. THERMAL MODEL

In the second step, the power deposited within the skin was used as a heat source in Pennes bioheat equation (3) using Bioheat Transfer module to determine the evolution of temperature with time

$$\rho C \frac{\partial T}{\partial t} = \nabla \cdot (k \nabla T) - \rho_b C_b \omega_b (T - T_b) + Q_m + PLD \tag{3}$$

where ρ is the density [kg · m^{-3}], C is the specific heat [J · kg^{-1}·°C^{-1}], k is the thermal conductivity [W · m^{-1}·°C^{-1}], Q_m is the metabolic heat [W · m^{-3}], t is time [s] and T is the temperature [°C]. Moreover, ρ_b is the blood density [kg · m^{-3}], C_b is the blood specific heat [J · kg^{-1}·°C^{-1}], ω_b is the blood flow rate [ml · s^{-1}·ml^{-1}] and T_b is the temperature [°C] of blood. In the absence of the experimental data on the temperature of blood in cutaneous capillaries, T_b was assumed to be 37 °C. The temperature of blood in cutaneous capillaries is expected to be slightly lower than the core body temperature (37 °C). Note that the blood perfusion was considered only in dermis (0.0014 ml · s^{-1}·ml^{-1}) [6] as stratum corneum and epidermis are avascular. However, blood perfusion in skin can be as high as 0.012 ml · s^{-1}·ml^{-1} [6]. The metabolic heat generation within skin (1620 W/m^3 under resting conditions) was neglected as it was insignificant (an order of magnitude smaller) with respect to heat deposited by mmWaves [27]. The first term on the right of (3) represents thermal conduction due to temperature gradients whereas the second term approximates the complicated three-dimensional

TABLE 2. Thermal Properties

Compartment	Water Content (%)	Thermal conductivity ($W \cdot m^{-1} \cdot °C^{-1}$)	Heat capacity ($J \cdot kg^{-1} \cdot °C^{-1}$)	Density ($kg \cdot m^{-3}$)
Stratum corneum [6]	5	0.2	2089.4	1200
Epidermis and Dermis [6], [29]	65-70	0.37	3391	1109
Blood [32]	83.8	0.49	3728.9	1056.7
Axoplasm [31]	89.5	0.53	3881.3	1036.75
Water [29]	100	0.6	4178	1000
Proteins [25], [39], [40]	0	0.18	2008	1350

phenomenon of heat loss due to blood flow in tissue by volumetrically distributed scaler heat sinks or sources. Although, more sophisticated mathematical models, which take into account tissue microvasculature, have been developed, the simplicity and remarkable agreement with experimental data has made Pennes bioheat equation the quantitative foundation for modeling bioheating [28]. Nevertheless, there is a general consensus now that the thermal equilibration between the blood and surrounding tissue does not take place in the capillary bed as assumed in Pennes bioheat model, but rather in post- and pre-capillary vessels [42]. Additionally, the perfusion rate is also assumed to be independent of temperature in Pennes bioheat model.

The thermal properties of the considered structures were derived from the literature [29] and are listed in Table 2. In the absence of available data on the thermal properties of cutaneous nerves, capillaries and stratum corneum, the following mixture equations [30] were used to approximate their thermal properties based on their water content [31], [32]. The water content of stratum corneum was obtained from [6], [33].

$$\rho_{mix} = \rho_p \phi_p + \rho_w \phi_w \tag{4}$$

$$C_{mix} = \frac{\rho_p \phi_p C_p + \rho_w \phi_w C_w}{\rho_p \phi_p + \rho_w \phi_w} \tag{5}$$

$$k_{mix} = \frac{k_w + 2k_p + 2\phi_w (k_w - k_p)}{k_w + 2k_p - \phi_w (k_w - k_p)} k_p \tag{6}$$

where ρ, ϕ, C and k are the density, volume fraction, heat capacity and thermal conductivity. The subscripts w, p and mix indicate the thermal properties of water, proteins and the mixture, respectively. The thermal conductivity, heat capacity, and density of the blood evaluated by mixture equation and reported in Table 2 is within the range provided in [29] (0.49–0.56 $W \cdot m^{-1} \cdot °C^{-1}$, 3300–3900 $J \cdot kg^{-1} \cdot °C^{-1}$, 1025–1060 $kg \cdot m^{-3}$). Due to lack of the reliable experimental data, the specific heat capacity and thermal conductivity of bound water were assumed to be similar to that of free water. The thermal conductivity and specific heat capacity of bound water are expected to be lower than that of free water because of its limited molecular mobility. Moreover, the thermal properties, blood perfusion and metabolic heat production were assumed to be independent of temperature because temperature elevation in skin under ICNIRP safety limits was found to be low (0.4 °C) [12].

The heat loss from skin surface to the environment due to convection, linearized radiation and evaporation was modeled as convective heat flux boundary condition based on Newton's law of cooling.

$$q_0 = h(T_{air} - T) \tag{7}$$

where q_0 is the heat flux, $h = 8.48\ W \cdot m^{-2} \cdot °C^{-1}$ [6] is the heat transfer coefficient (1-15 $W \cdot m^{-2} \cdot °C^{-1}$) [15] at the skin surface and T_{air} is the temperature of the air at the skin surface assumed to be 20 °C. The thermal insulation $[n \cdot (k \nabla T) = 0]$ boundary conditions were applied in ±x and ±y because lateral heat transport was found to be an order of magnitude less than heat conduction in the direction normal to the skin surface in most exposure scenarios involving mmWaves [34]. Lastly, a constant temperature of 35 °C was fixed at the base of the dermis [35].

The baseline steady state temperature distribution within the skin due to natural heat sources (convective boundary condition and blood perfusion) was used as an initial condition for subsequent transient simulations in which mmWave heat source was turned on. The temperature increment (ΔT) within cutaneous nerve and capillary was calculated as the difference of the absolute temperatures with and without mmWave heating.

1) THERMAL DAMAGE

Thermal damage was estimated by using Arrhenius model, which takes into account the cumulative effect of elevated temperature and exposure time on tissue damage.

$$\Omega = \int_0^t A\, exp\left(\frac{-E_a}{RT}\right) dt \tag{8}$$

where Ω is the damage index [dimensionless], A is the frequency factor [s^{-1}], E_a is the activation energy [$J \cdot mole^{-1}$], R is the universal gas constant [8.314 $J \cdot mole^{-1} \cdot °C^{-1}$], T is temperature [°C] and t is the exposure duration [s]. The frequency factor and activation energy of skin (epidermis and dermis) were adopted from a recent study by Foster [15]. Due to lack of aforementioned data for cutaneous nerves, capillaries and stratum corneum, the frequency factor and activation energy of skin were used as a first approximation. The damage index ($\Omega = 1$) was assumed to be the critical threshold for tissue damage which corresponds to denaturation of 63% of molecules [36].

D. NUMERICAL METHOD

The electrothermal computational domain was discretized non-uniformly by roughly $2.2 \times 10^5 - 2.7 \times 10^5$ second-order tetrahedral finite mesh elements. The edge lengths of the smallest mesh elements within the nerve, capillary and dermis were 0.5 μm, 1 μm, and 40 μm, respectively. The resulting algebraic equations due to finite element approximation were solved using an implicit time stepping

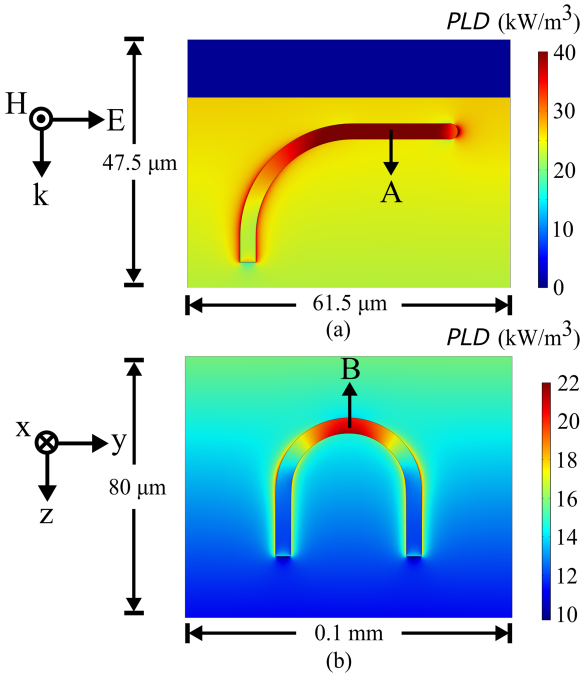

FIGURE 2. ***PLD*** **distribution for** ***IPD*** **= 10 W/m² at 60 GHz: (a) Aδ nerve fiber; (b) capillary loop.**

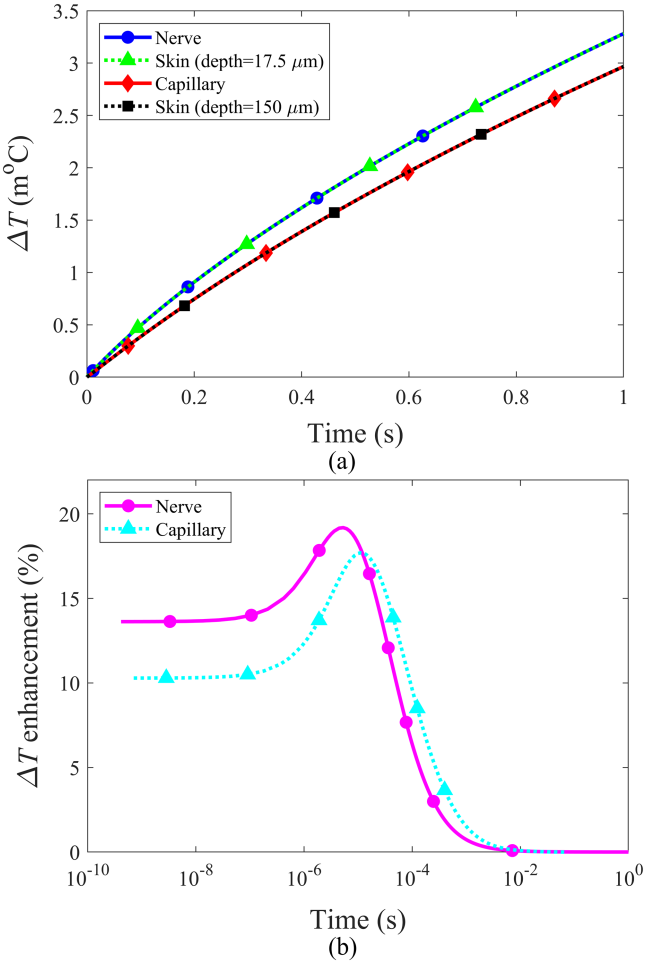

FIGURE 3. **(a) Time course of ΔT within nerve, capillary and surrounding skin; (b) ΔT enhancement within nerve and capillary. (*IPD* = 10 W/m² at 60 GHz).**

scheme. The initial step was 0.4 ns and subsequent time steps were automatically controlled by time dependent solver (maximum time step=1.8 ms). The relative tolerance of the time dependent solver was set to 10^{-9}. The simulations were run on a workstation equipped with Intel(R) Xeon CPU (E5-2687 W v3 @ 3.1 GHz) and 256 GB RAM.

III. RESULTS

A. ABSORBED ELECTROMAGNETIC POWER

Fig. 2 depicts that the electromagnetic power was preferentially absorbed within the leading segment of the epidermal nerve and capillary loop compared to the surrounding skin at 60 GHz. The maximal *PLD* within the nerve (41.6 kW/m^3) and the capillary loop (20.75 kW/m^3) was 37.3% and 30.2% higher compared to the surrounding skin for an *IPD* of 10 W/m^2, respectively. The power losses within the nerve and the capillary loop were higher not only due to their higher water content compared to the surrounding skin but also because incident electric field was tangential to their leading segments. The *PLD* enhancement within simplified models of the nerve and the capillary loop presented here was almost similar (difference $< 0.6\%$) to that within more detailed models given in [25].

B. TRANSIENT MMWAVE-INDUCED HEATING

1) CONTINOUS EXPOSURE

Fig. 3(a) shows the time course of temperature elevation above initial temperature distribution at the maximal *PLD* in points A and B (Fig. 2) located at the center of the nerve and capillary loop. The ΔT curves in Fig. 3(a) can be divided into two main periods. During the first 0.2 s, the ΔT within the nerve (4.55 m°C/s) and capillary loop (3.7 m°C/s) increased almost linearly with time. This initial linear period was followed by roughly an exponential period (0.2 s–1 s) where the rate of temperature rise within the nerve (3 m°C/s) and capillary loop (2.8 m°C/s) slowed down. The decrease in slope $d(\Delta T)/dt$ of the ΔT curves is due to the dissipation of the absorbed power within the nerve and capillary loop by heat conduction. Note that $d(\Delta T)/dt$ of nerves is higher than that of the capillary loop because of higher *PLD* and higher thermal diffusivity $(k/C\rho)$ of the nerve (1.32×10^{-7} m^2/s) compared to the capillary loop (1.24×10^{-7} m^2/s).

Since, the difference of ΔT between the nerve and surrounding skin was too small (several n°C) to be discerned in Fig. 3(a), this difference was plotted in terms of normalized percentage $[(\Delta T_{nerve} - \Delta T_{skin})/\Delta T_{nerve} \times 100\%]$ in Fig. 3(b). Initially, between a brief period of 0.1 μs $-$ 5 μs (nerve) and 0.1 μs $-$ 10 μs (capillary), the ΔT enhancement within the nerve (14%$\rightarrow$19.2%) and the capillary loop (10.7%$\rightarrow$17.7%) increased almost linearly compared to the

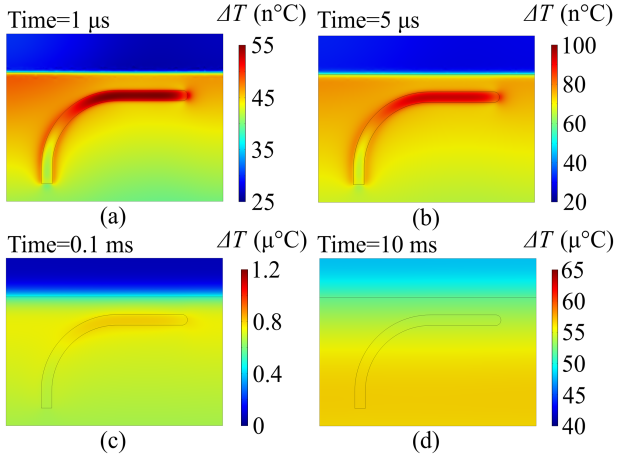

FIGURE 4. ΔT distribution within nerve for *IPD* = 10 W/m^2 at 60 GHz: (a) 1 μs; (b) 5 μs; (c) 0.1 ms; (d) 10 ms.

surrounding skin. The ΔT enhancement linearly increased because the heat transfer due to thermal conduction was negligible in this early transient period. In other words, ΔT enhancement was proportional to local *PLD* between roughly 0.1 μs and 5 μs. Note that ΔT enhancement within the nerve was slightly higher (1.5%) than in the capillary loop due to higher *PLD* within the nerve.

Fig. 3(b) also shows that the maximal ΔT enhancement within the capillary loop was delayed by 5 μs compared to the maximal ΔT enhancement within the nerve. This delay was due to lower thermal conductivity of the blood (0.49 W $\cdot$ m$^{-1}\cdot$°C^{-1}) in comparison to the nerve (0.53 W $\cdot$ m$^{-1}\cdot$°C^{-1}), which more slowly decreased the temperature gradient between the blood and surrounding skin.

Between 5 μs–10 ms and 10 μs–10 ms, the ΔT enhancement within the nerve (19.2%$\rightarrow$0.06%) and capillary loop (17.7%$\rightarrow$0.09%) decreased gradually compared to the surrounding skin. This was because the thermal diffusion equalized the temperature gradient between the nerve, capillary loop and surrounding skin. Stated differently, the steady-state temperature field was established within the nerve and capillary loop after 10 ms of continuous mmWave-induced heating.

The spatial distribution of temperature elevation within nerve at 1 μs, 5 μs, 0.1 ms and 10 ms is shown in Fig. 4. Fig. 4(a) reveals local concentration of heating within the leading segment of the nerve. At 1 μs, the ΔT within the nerve (55.01 n°C) was 16.5% higher than the surrounding skin (45.9 n°C). Note that at 1 μs the temperature distribution is almost identical to *PLD* distribution in Fig. 2(a). This is because *PLD* distribution represents instantaneous heating of the nerve. The leading horizontal segment of the nerve continued to retain heat (93.3 n°C) until 5 μs. The aforementioned temperature transients are minuscule because of weak incident power levels (10 W/m^2) applied for a very brief period.

The higher temperature (93.3 n°C) within the nerve in comparison to the surrounding skin (75.4 n°C) at 5 μs established a temperature gradient. This led to heat transfer via conduction as heat flows from the heated nerve to surrounding skin with a low temperature. Fig. 4(c) displays the diffused temperature pattern at 0.1 ms due to heat conduction. The ΔT within nerve (0.8 μ°C) at 0.1 ms is 6.21% higher compared to surrounding skin (0.74 μ°C).

Finally, the nerve heating reached the steady state at 10 ms as shown in Fig. 4(d). The difference of ΔT between nerve (53.99 μ°C) and surrounding skin (53.96 μ°C) was only 0.06% at 10 ms. This is because at 10 ms the amount of power flowing out of the nerve surface due to thermal conduction to the surrounding skin was equal to the power deposited by mmWave within the nerve. The characteristic time for the nerve to reach the steady state with the surrounding skin was small (10 ms) because of small dimensions (diameter= 3 μm) of the nerve. In other words, small nerve possessed larger surface area per unit volume, which led to faster dissipation of heat to the surrounding skin by thermal conduction. The phenomenon of nanoscale tissue heating was discussed in detail by Rabin [37] and Keblinski [38] in context of nanoparticle heating. Note that only nerve has reached thermal equilibrium with skin at 10 ms. Clearly, the surrounding skin will take more time to reach steady state due to mmWave exposure [21].

The effect of diameter of the epidermal nerve fibers on temperature distribution was also examined because, in addition to aforementioned Aδ fibers (3 μm), the epidermis also contains C-fibers (1 μm). The maximal ΔT within the C-fiber (51.2 n°C) occurred at 2 μs and was only 7.7% higher than the surrounding skin (47.25 n°C). In other words, the Aδ fibers retain 45.1% more heat for 60% longer time in comparison to C-fibers. The swift clearance of heat from C-fiber was because it represented a smaller heat source with higher surface area to volume ratio compared to Aδ fiber. The C-fiber (3 ms) also more quickly (70% faster) achieved thermal equilibrium with the surrounding skin than Aδ fiber (10 ms).

Fig. 4 also shows temperature gradient between the stratum corneum and epidermis. At 0.1 ms, the ΔT in the stratum corneum (89.1 n°C) was 87.97% lower than nearby skin. This was because of 95.3% lower *PLD* in stratum corneum (1.2 kW/m^2) compared to the adjacent skin. In the absence of the stratum corneum, the maximal ΔT within the nerve at 0.1 ms was only increased by 0.31%. This suggested that stratum corneum was not effective to inhibit heat exchange between nerve and cooler surrounding environment.

Fig. 5 illustrates the differential temperature increment within the capillary loop at four-time instants (1 μs, 10 μs, 0.1 ms and 10 ms) for the electric field tangential to the leading segment of the capillary. The first striking observation was regarding the presence of a hot spot (region of highest temperature=42.02 n°C) in the leading segment of the capillary loop at 1 μs. The ΔT within the capillary loop at 1 μs was 12.74% higher than in the surrounding skin (36.66 n°C). This is in contrast to the commonly used homogeneous skin models for mmWave dosimetry in which temperature maxima occurs at the skin surface. The selective heating (90.7 n°C) of the top portion of the capillary loop continued until 10 μs. The hot spots within the capillary loop (0.47 μ°C) began to

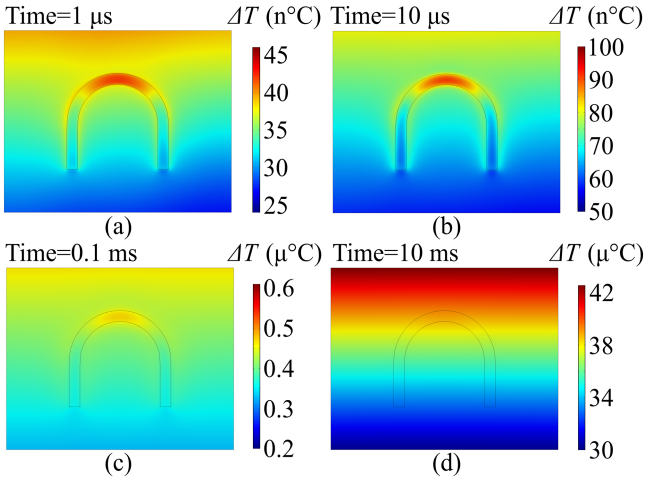

FIGURE 5. ΔT distribution within capillary for $IPD = 10$ W/m^2 at 60 GHz: (a) 1 μs; (b) 5 μs; (c) 0.1 ms; (d) 10 ms.

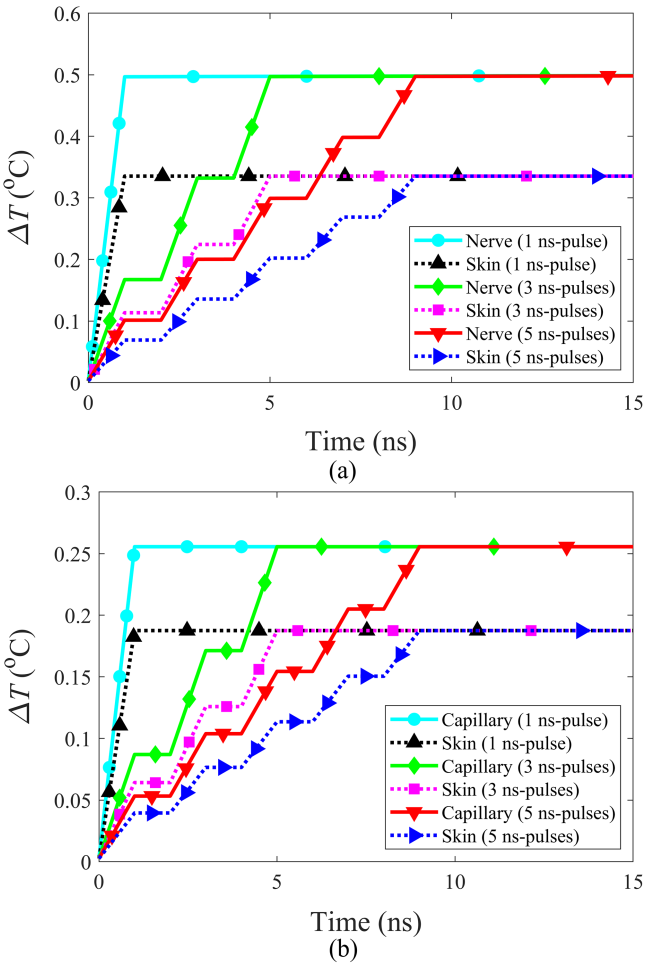

FIGURE 6. ΔT for 1 ns, 3 ns and 5 ns mmWave pulses with constant fluence of 0.48 kJ/m^2 ($IPD = 480$ GW/m^2, 160 GW/m^2 and 96 GW/m^2): (a) nerve; (b) capillary.

blur compared to the surrounding skin (0.42 μ°C) at around 0.1 ms due to heat conduction. By 10 ms, thermal conduction cleared remaining heat from the capillary loop and transferred it to the surrounding skin. The difference in ΔT between the capillary loop (38.95 μ°C) and surrounding skin (38.92 μ°C) was 0.09% at 10 ms. This indicated a balance between the heat input into the capillary loop by mmWave exposure and heat removal to surrounding skin due to thermal conduction at 10 ms. In other words, at thermal equilibrium there was no net heat exchange between the capillary loop and the surrounding skin.

It is worthwhile to mention that the heat flow to the environment modeled by convection boundary condition suppressed the temperature enhancement within the nerve (17.1%) and the capillary loop (15.8%) before 0.1 μs compared to the case when thermal insulation boundary condition was applied on the skin surface. Similarly, the temperature enhancement within the nerve also increased (20%) with its depth (16-99.5 μm) in epidermis due to diminished effect of air cooling and because the *PLD* enhancement within the nerve compared to the surrounding skin remained constant with depth. Furthermore, the effect of blood perfusion on the aforementioned ΔT enhancement within the nerve and the capillary loop was negligible (less than 0.2%). This was because the temperature transients caused by continuous mmWave heating were small and the blood perfusion can only remove the heat from the skin if the temperature of skin is higher than blood temperature (37 °C).

2) PULSED EXPOSURE

It is clear from the aforementioned results that continuous heating induced by mmWaves at *IPD* of 10 W/m^2 cannot produce biologically significant temperature elevations within the nerve and capillary loop inside the skin. One way to achieve localized heating is to push the maximum energy (fluence=0.48 kJ/m^2 at 60 GHz) permitted under ICNIRP guidelines into the nerve and the capillary loop at faster time scales than the those required for the heat to diffuse to the surrounding skin. Fig. 6 shows the time evolution of temperature elevation inside the nerve and the capillary loop for one ($IPD = 480$ GW/m^2), three ($IPD = 160$ GW/m^2) and five ($IPD = 96$ GW/m^2) nano-second mmWave pulses. The ΔT for a single nano-second pulse increased linearly with time whereas for three and five nano-second pulses ΔT rose in a stairstep fashion. The maximal ΔT in the nerve (0.5 °C) and the capillary loop (0.25 °C) at the end (10 ns) of all applied pulse trains was 34% and 24% higher than in the surrounding skin. Note that the maximal ΔT within the nerve was 50% higher than in the capillary loop because the maximal *PLD* in the former was also roughly 50% higher than the latter. Fig. 6 also shows that when mmWave pulses were switched off, ΔT within the nerve and the capillary loop had a constant difference with ΔT in the surrounding skin because the heat transport due to conduction was negligible at nano-second time scales.

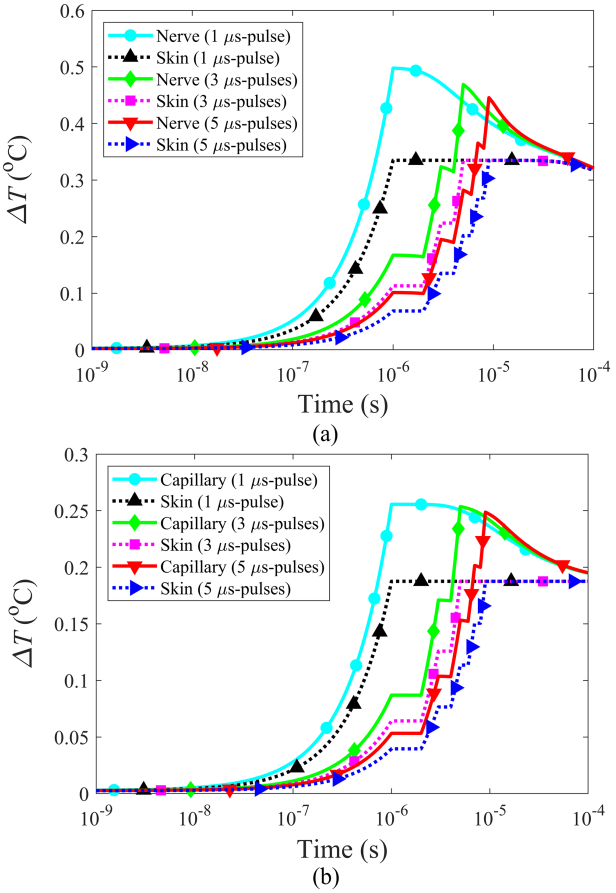

FIGURE 7. ΔT for 1 μs, 3 μs and 5 μs-mmWave pulses with constant fluence of 0.48 kJ/m^2 (*IPD* = 480 MW/m^2, 160 MW/m^2 and 96 MW/m^2): (a) nerve; (b) capillary.

Although, the maximal ΔT in the nerve and capillary loop was similar for one, three and five nano-second pulses because the same amount of total energy was deposited in all three cases, the heating rates of the nerve (0.5 °C/ns) and the capillary loop (0.25 °C/ns) for a single nano-second pulse were 89.4% and 88.9% faster than five nano-second pulses. Moreover, despite the higher specific heat of the nerve and capillary loop compared to skin, the rate of ΔT rise in the nerve and capillary loop due to a single mmWave nano-second pulse was 34% and 26% higher than surrounding skin. This was because in absence of heat conduction at nano-second time scales, slope of ΔT curves were directly proportional to the nerve and capillary loop *PLD*, which was higher than that of skin.

Fig. 7 displays the time course of ΔT inside the nerve and the capillary loop for one (*IPD* = 480 MW/m^2), three (*IPD* = 160 MW/m^2) and five (*IPD* = 96 MW/m^2) micro-second mmWave pulses. For a single micro-second mmWave pulse, ΔT within the nerve and capillary loop increased almost linearly with time. The maximal ΔT within the nerve (0.5 °C) and the capillary loop (0.25 °C) at 1 μs was 34% and 24% higher than the surrounding skin. On the other hand, for three and five micro-second mmWave pulses, the nerve and capillary loop periodically warmed up when the mmWave power was switched on and cooled down when the mmWave power was turned off as displayed in Fig. 7. Between 3 μs to 4 μs, the nerve and capillary cooled down by 8.7 m°C and 0.7 m°C respectively. In other words, after the application of second micro-second mmWave pulse, the nerve cooled 91.9% more rapidly than the blood capillary. This was because of smaller size (36.8%) and higher thermal diffusivity (6%) of nerve compared to the capillary loop. Fig. 7 also shows that, in contrast to the nano-second mmWave pulses, the peaks of ΔT in the nerve and capillary loop due to three and five micro-second mmWave pulses were smaller than corresponding ΔT peaks for a single micro-second pulse. The ΔT peaks in the nerve (0.446 °C) and the capillary loop (0.249 °C) due to five micro-second mmWave pulses were 10.5% and 2.7% smaller than ΔT peak for a single micro-second mmWave pulse. The ΔT peaks for multiple micro-second pulses were smaller than those of multiple nano-second pulses because there was sufficient time for the heat diffusion to the surrounding skin in the former case.

Lastly, after pulsed exposure, ΔT within the nerve and blood capillary decreased almost exponentially to ΔT in the surrounding skin. At 0.1 ms, the difference in ΔT within the nerve and the surrounding skin was 3.1 m°C whereas the difference in ΔT within the blood capillary and surrounding skin was 7.5 m°C. Moreover, the ΔT curves in Fig. 7 are also asymmetrical because the heating of the nerve and capillary loop due to micro-second mmWave pulses were faster than their cooling. For instance, for a single micro-second mmWave pulse, the heating of nerve and capillary loop were roughly two orders of magnitude faster than their subsequent cooling. The aforementioned results suggest that multiple nano-second mmWave pulses lead not only to more localized heating within the nerve and the capillary loop compared to multiple micro-second mmWave pulses, but also result in higher ΔT maxima and cause more rapid rate of heating. Although, the maximal ΔT in the nerve and the capillary loop due to pulsed mmWave exposure was six orders of magnitude higher than that for continuous mmWave exposure, the maximal ΔT in the nerve and the capillary loop was 90% and 95% lower than current 5 °C limit set by ICNIRP guidelines. Note that the aforementioned high *IPD* are the most extreme exposure parameters permitted under current ICNIRP guidelines and are not representative of exposure from wireless devices such as cellular phones.

3) THERMAL DAMAGE

The possibility of using brief (3 μs) high power (*IPD* = 13.4 GW/m^2) pulses to selectively burn the epidermal nerves while sparing the surrounding skin is considered in this section. Fig. 8(a) shows that temperature within the nerve (36.05–75.9 °C) and the surrounding skin (36.05-63.91 °C) increased and decreased in large fluctuations on application of ten aforementioned pulses separated by a cooling period of 10 s. The heating rate was seven orders of magnitude faster than the

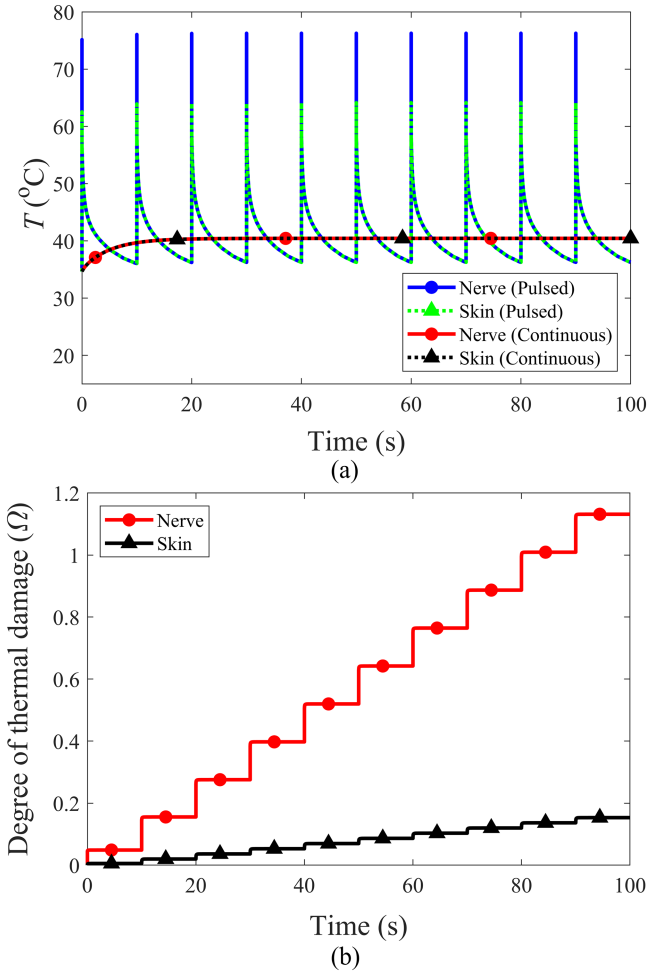

FIGURE 8. **(a) Time course of temperature within nerve and surrounding skin due to continuous (*IPD* = 4.02 kW/m^2) and pulsed (ten 3 μs-pulses with *IPD* = 13.4 GW/m^2 separated by a cooling period of 10 s each) exposure at 60 GHz; (b) thermal damage within nerve and surrounding skin calculated for 10 s periods.**

cooling rate due to high energy pulses. Note that the maximum temperature increased only to 40.44 °C due to equivalent continuous mmWave exposure ($IPD = 4.02$ kW/m^2).

Fig. 8(b) shows that at the end of 100 s, the nerve was irreversibly damaged ($\Omega = 1.1$) while sparing the surrounding skin ($\Omega = 0.15$). Note that the Arrhenius damage index $\Omega = 1$ corresponds to denaturation of 63% of the molecules. The thermal damage within the nerve roughly increased with an increment of $\Omega = 0.11$ after each pulse and associated cooling phase. Roughly 62.5% of the thermal damage accumulated within the nerve during the application of mmWave pulse whereas 37.5% of the damage occurred during the cooling phase. The nerve continued to receive thermal dose after mmWave power was turned off due to the integral relation between temperature and thermal dose. Although, the maximum temperature difference between the nerve and the surrounding skin was only 11.9 °C, the nerve was preferentially damaged because the thermal dose increases hyperbolically with temperature and linearly with time.

IV. CONCLUSION

This paper presents, for the first time, the microthermal analysis of cutaneous nerves and capillaries exposed to continuous and pulsed 60 GHz radiation. The maximum mmWave induced heating of nerve (93.3 n°C) and capillary (90.7 n°C) occurred after respectively 5 μs and 10 μs of continuous exposure at 10 W/m^2 and was 19.2% and 17.7% higher than in the surrounding skin. The preferential heating of nerve and capillary ended after 10 ms of continuous exposure due to rapid diffusion of heat from microscale nerve and capillary to the surrounding skin. This suggests that local temperature fluctuations induced by continuous mmWaves within nerve and capillary are biologically insignificant even though the nerve (41.6 kW/m^3) and capillary (20 kW/m^3) absorbed respectively 37.3% and 30.2% more electromagnetic power per unit volume compared to the surrounding skin.

In contrast, the maximum temperature elevation within the nerve (0.5 °C) and capillary (0.25 °C) due to the brief (nanosecond and microsecond) high fluence mmWave pulses (0.48 kJ/m^2 at 60 GHz) permitted by the ICNIRP guidelines was 34% and 24% higher than in the surrounding skin. In other words, the high-water content skin substructures with microscale dimensions can be heated locally by supplying energy into them at the time scales faster than those required for heat to dissipate to the surrounding skin. Although, nerve terminations were not modeled in this study due to lack of geometrical data, they are expected to retain more mmWave induced heat for a longer period of time compared to the rest of the nerve fiber due to their slightly larger size.

A sequence of ten 13.4 GW/m^2 microsecond pulses at 60 GHz separated by 10 s of cooling period were used to demonstrate the possibility to selectively burn the portion of the nerve parallel to the applied E field [damage index (Ω)=1.1)] without damaging the surrounding skin ($\Omega = 0.15$). Note that the objective of the aforementioned results was not to provide a definite value of *IPD* to selectively damage the nerves within skin, but to demonstrate the possibility of such a selective thermal damage.

It is worth to mention that although high-powered ($\approx$ GW/m^2) pulsed ($\approx \mu$s) mmWave sources are currently not available, the widespread adoption of mmWave technology might lead to the development of high-powered pulsed mmWave sources, which could be utilized for potential medical applications. Further optimization studies are also required to ascertain that upper limit of mmWave *IPD* is below the threshold for dielectric breakdown of air (3 MV/m) [48] and thermoacoustically induced pain [49]. Moreover, $\Omega = 1.1$ within the nerve was calculated based on the assumed electromagnetic and thermal properties, and it can be further refined by using more accurate electromagnetic and thermal parameters. In addition, since the temperature dependence of physical properties and thermoregulatory mechanisms (vasodilation and sweating) were neglected, the results should be considered as a worst-case scenario.

Even though, the proposed model provides insights into mmWave-induced heating at the microscale level within the

skin, it can be further improved by incorporating natural variability in electromagnetic and thermal properties of cutaneous nerves and blood vessels. Lastly, in future it will be important to perform a sensitivity analysis which takes into account variability in cutaneous blood perfusion rate depending on the body regions.

Finally, one possible extension of this work would be taking into account the possible effect of those modest temperature rises on the activity of those nerves: it is indeed well-known that temperature is a key factor of the membrane resting potential (Nernst potential), therefore using biomathematical models of the nerve membrane potential in response to those temperature changes might be informative in terms of neurophysiological responses. Such approach would have the benefit to provide an integrated view coupling dosimetry with potential neurophysiological effects.

REFERENCES

[1] A. Alhamed, O. Kazan, G. Gültepe, and G. M. Rebeiz, "Multi-band/multistandard 15-57 GHz receive phased-array module based on 4 x 1 beamformer IC and supporting 5 G NR FR2 operation," *IEEE Trans. Microw. Theory Techn.*, vol. 70, no. 3, pp. 1732–1744, Mar. 2022.

[2] Y. Zhang, W. Yang, Q. Xue, J. Huang, and W. Che, "Broadband dual-polarized differential-fed filtering antenna array for 5G millimeter-wave applications," *IEEE Trans. Antennas Propag.*, vol. 70, no. 3, pp. 1989–1998, Mar. 2022.

[3] J. Guo, Y. Hu, and W. Hong, "45° polarized wideband and wide-coverage patch antenna array for millimeter-wave communication," *IEEE Trans. Antennas Propag.*, vol. 70, no. 3, pp. 1919–1930, Mar. 2022.

[4] H. T. Chou, Z. H. Lin, D. B. Lin, C. S. Yang, P. Z. Shen, and C. L. Pan, "Considerations of dielectric property deviation and mechanical limitations for antenna-in-package fabrication by SiP-based stacked organic dielectric substrates at millimeter-wave frequencies," *IEEE Trans. Antennas Propag.*, vol. 70, no. 2, pp. 1309–1319, Feb. 2022.

[5] C. Wu et al., "Millimeter-wave waveguide-to-microstrip inline transition using a wedge-waveguide IRIS," *IEEE Trans. Microw. Theory Techn.*, vol. 70, no. 2, pp. 1087–1096, Feb. 2022.

[6] M. C. Ziskin, S. I. Alekseev, K. R. Foster, and Q. Balzano, "Tissue models for RF exposure evaluation at frequencies above 6 GHz," *Bioelectromagnetics*, vol. 39, no. 3, pp. 173–189, 2018.

[7] International Commission on Non-Ionizing Radiation Protection and others, "Guidelines for limiting exposure to electromagnetic fields (100 kHz to 300 GHz)," *Health Phys.*, vol. 118, no. 5, pp. 483–524, 2020.

[8] H. H. Pennes, "Analysis of tissue and arterial temperature in the resting human forearm," *J. Appl. Physiol.*, vol. 1, pp. 93–122, 1948.

[9] A. Hirata et al., "Human exposure to radiofrequency energy above 6 GHz: Review of computational dosimetry studies," *Phys. Med. Biol.*, vol. 66, no. 8, Apr. 2021, Art. no. 08TR01.

[10] A. Kanezaki, A. Hirata, S. Watanabe, and H. Shirai, "Parameter variation effects on temperature elevation in a steady-state, one-dimensional thermal model for millimeter wave exposure of one- and three-layer human tissue," *Phys. Med. Biol.*, vol. 55, pp. 4647–4659, 2010.

[11] K. Sasaki, K. Wake, and S. Watanabe, "Monte Carlo simulations of skin exposure to electromagnetic field from 10 GHz to 1 THz," *Phys. Med. Biol.*, vol. 62, no. 17, pp. 6993–7010, Aug. 2017.

[12] A. Christ, T. Samaras, E. Neufeld, and N. Kuster, "RF-induced temperature increase in a stratified model of the skin for plane-wave exposure at 6-100 GHz," *Radiat. Protection Dosimetry*, vol. 188, no. 3, pp. 350–360, Mar. 2020.

[13] S. I. Alekseev, A. A. Radzievsky, I. Szabo, and M. C. Ziskin, "Local heating of human skin by millimeter waves: Effect of blood flow," *Bioelectromagnetics*, vol. 26, no. 6, pp. 489–501, Sep. 2005.

[14] K. R. Foster, M. C. Ziskin, and Q. Balzano, "Thermal response of human skin to microwave energy: A critical review," *Health Phys.*, vol. 111, no. 6, pp. 528–541, Dec. 2016.

[15] K. R. Foster, M. C. Ziskin, Q. Balzano, and A. Hirata, "Transient thermal responses of skin to pulsed millimeter waves," *IEEE Access*, vol. 8, pp. 130239–130251, Jul. 2020.

[16] M. Zhadobov et al., "Millimeter waves as a source of selective heating of skin," *Bioelectromagnetics*, vol. 36, no. 6, pp. 464–475, Sep., 2015.

[17] G. Sacco, S. Pisa, and M. Zhadobov, "Age-dependence of electromagnetic power and heat deposition in near-surface tissues in emerging 5G bands," *Sci. Rep.*, vol. 11, 2021, Art. no. 3983.

[18] G. Sacco, S. Pisa, and M. Zhadobov, "Impact of textile on electromagnetic power and heating in near-surface tissues at 26 GHz and 60 GHz," *IEEE J. Electromagn., RF Microw. Med. Biol.*, vol. 5, no. 3, pp. 262–268, Sep. 2021.

[19] C. Leduc, M. Zhadobov, and R. Sauleau, "Thermal model of a tissue equivalent phantom at millimeter waves," *IEEE Trans. Microw. Theory Techn.*, vol. 65, no. 3, pp. 1036–1045, Jan. 2017.

[20] K. Sasaki et al., "Design of a skin equivalent phantom for estimating surface temperature elevation due to human exposure to electromagnetic fields from 10 to 100 GHz," *IEEE Trans. Electromagn. Compat.*, vol. 63, no. 5, pp. 1631–1639, Oct. 2021.

[21] R. Morimoto, A. Hirata, I. Laakso, M. C. Ziskin, and K. R. Foster, "Time constants for temperature elevation in human models exposed to dipole antennas and beams in the frequency range from 1 to 30 GHz," *Phys. Med. Biol.*, vol. 62, no. 5, pp. 1676–1699, Feb. 2017.

[22] I. Laakso, R. Morimoto, J. Heinonen, K. Jokela, and A. Hirata, "Human exposure to pulsed fields in the frequency range from 6 to 100 GHz," *Phys. Med. Biol.*, vol. 62, no. 17, pp. 6980–6992, 2017.

[23] G. Shafirstein and E. G. Moros, "Modelling millimetre wave propagation and absorption in a high resolution skin model: The effect of sweat glands," *Phys. Med. Biol.*, vol. 56, no. 5, pp. 1329–1339, Mar. 2011.

[24] K. R. Foster, "Comments on Betzalel The human skin as a sub-THz receiver-does 5 G pose a danger to it or not?," *Environ. Res.*, vol. 183, pp. 109008–109008, Apr. 2020.

[25] Z. Haider, Y. Le Dréan, G. Sacco, D. Nikolayev, R. Sauleau, and M. Zhadobov, "High-resolution model of human skin appendages for electromagnetic dosimetry at millimeter waves," *IEEE J. Microwaves*, vol. 2, no. 1, pp. 214–227 , Jan. 2022.

[26] R. Kanawade et al., "Novel method for early signs of clinical shock detection by monitoring blood capillary/vessel spatial pattern," *J. Biophoton.*, vol. 7, no. 10, pp. 841–849, Oct. 2014.

[27] T. Samaras, A. Christ, A. Klingenbock, and N. Kuster, "Worst case temperature rise in a one-dimensional tissue model exposed to radiofrequency radiation," *IEEE Trans. Biomed. Eng.*, vol. 54, no. 3, pp. 492–496, Mar. 2007.

[28] H. Arkin, "Recent developments in modeling heat transfer in blood perfused tissues," *IEEE Trans. Biomed. Eng.*, vol. 41, no. 2, pp. 97–107, Feb. 1994.

[29] "IT'IS foundation dielectric properties database," Sep. 2020. [Online]. Available: https://itis.swiss/virtual-population/tissue-properties/database/dielectric-properties/

[30] S. Zheng, H. S. Fogler, and A. Haji-Akbari, "A fundamental wax deposition model for water-in-oil dispersed flows in subsea pipelines," *AIChE J.*, vol. 63, no. 9, pp. 4201–4213, Sep. 2017.

[31] W. J. Adelman Jr., J. M. Arnold, and D. L. Gilbert, *Squid as Experimental Animals*. New York, NY, USA: Springer, 2013, pp 235–302.

[32] P. D. Maskell, A. W. Jones, S. B. Heymsfield, S. Shapses, and A. Johnston, "Total body water is the preferred method to use in forensic blood-alcohol calculations rather than Ethanol's volume of distribution," *Forensic Sci. Int.*, vol. 316, Nov. 2020, Art. no. 110532.

[33] A. Y. Sdobnov, M. E. Darvin, J. Schleusener, J. Lademann, and V. V. Tuchin, "Hydrogen bound water profiles in the skin influenced by optical clearing molecular agents—Quantitative analysis using confocal Raman microscopy," *J. Biophoton.*, vol. 12, no. 5, pp. 1–11, May 2019.

[34] K. R. Foster, H. Zhang, and J. M. Osepchuk, "Thermal response of tissues to millimeter waves: Implications for setting exposure guidelines," *Health Phys.*, vol. 99, no. 6, pp. 806–810, 2010.

[35] N. Prieto, M. E. Dugan, M. Juárez, Ó. López-Campos, R. T. Zijlstra, and J. L. Aalhus, "Using portable near-infrared spectroscopy to predict pig subcutaneous fat composition and iodine value," *Can. J. Animal Sci.*, vol. 98, no. 2, pp. 221–229, Oct. 2017.

[36] J. Zhou, J. K. Chen, and Y. Zhang, "Simulation of laser-induced thermotherapy using a dual-reciprocity boundary element model with dynamic tissue properties," *IEEE Trans. Biomed. Eng.*, vol. 57, no. 2, pp. 238–245, Aug. 2009.

[37] Y. Rabin, "Is intracellular hyperthermia superior to extracellular hyperthermia in the thermal sense?," *Int. J. Hypertherm.*, vol. 18, pp. 194–202, 2002.
[38] P. Keblinski, D. G. Cahill, A. Bodapati, C. R. Sullivan, and T. A. Taton, "Limits of localized heating by electromagnetically excited nanoparticles," *J. Appl. Phys.*, vol. 100, pp. 054305-1–054305-5, Sep. 2006.
[39] M. S. Baghe-Khandan and M. R. Okos, "Effect of cooking on the thermal conductivity of whole and ground lean beef," *J. Food Sci.*, vol. 46, no. 5, pp. 1302–1305, Sep. 1981.
[40] H. A. Shehadeh et al., "A mathematical model for meat cooking," Aug. 2019, *arXiv:1908.10787*.
[41] *IEEE Standard for Safety Levels With Respect to Human Exposure to Electric, Magnetic, and Electromagnetic Fields, 0 Hz to 300 GHz*, IEEE Std C95.1-2019 (Revision of IEEE Std C95.1-2005/ Incorporates IEEE Std C95.1-2019/Cor 1-2019), Oct. 4, 2019, pp. 1–312, doi: 10.1109/IEEESTD.2019.8859679.
[42] M. E. Kowalski and J. M. Jin, "Model-based optimization of phased arrays for electromagnetic hyperthermia," *IEEE Trans. Microw. Theory Tech.*, vol. 52, no. 8, pp. 1964–1977 , Aug. 2004.
[43] W. R. Kennedy and G. Wendelschafer-Crabb, "The innervation of human epidermis," *J. Neurol. Sci.*, vol. 115, no. 2, pp. 184–190, Apr. 1993.
[44] R. P. Arthur and W. B. Shelly, "The innervation of human epidermis," *J. Invest. Dermatol.*, vol. 32, no. 3, pp. 397–411, Mar. 1959.
[45] I. M. Braverman, "Ultrastructure and organization of the cutaneous microvasculature in normal and pathologic states," *J. Invest. Dermatol.*, vol. 93, no. 2, pp. 2S–9S, Aug. 1989.
[46] A. Lametschwandtner and O. Staindl, "The vascular architecture of the keloid: A scanning electron microscope study on vascular corrosion casts," in *Wound Healing and Skin Physiology*. Berlin, Heidelberg: Springer, 1995, pp. 137–151.
[47] W. Montagna, A. M. Kligman, and K. S. Carlisle, *Atlas of Normal Human Skin*. Philadelphia, PA, USA: Springer, 2012, pp. 155–175.
[48] T. C. Marshall, M. P. McCarthy, and W. D. Rust, "Electric field magnitudes and lightning initiation in thunderstorms," *J. Geophys. Res.*, vol. 100, pp. 7097–7103, 1995.
[49] K. R. Foster, D. C. Garrett, and M. C. Ziskin, "Can the microwave auditory effect be 'weaponized'?," *Front. Public Health*, vol. 9, Dec. 2021, Art. no. 788613.

ZAIN HAIDER received the Ph.D. degree in electronics from the Institute of Electronics and Telecommunications of Rennes, University of Rennes 1, Rennes, France, in 2022. He is currently a Postdoctoral Fellow with IETR. His research interests include microdosimetry, near-field to far-field transformation, hyperthermia, and metamaterials.

JULIEN MODOLO (Member, IEEE) received the M.Sc. degree in astrophysics and the Ph.D. degree in cognitive science from Bordeaux University, Bordeaux, France, in 2005 and 2008, respectively, and the Habilitation à Diriger des Recherches degree from Rennes University, Rennes, France, in 2019.

He was a Postdoctoral Fellow and then Principal Investigator with Lawson Health Research Institute, London, ON, Canada, before joining INSERM (Institut National de la Santé et de la Recherche Médicale) in 2015 as a full-time Scientist. His research interests include the fundamental mechanisms of interaction between electromagnetic fields and the central nervous system, and their implications for public health along with diagnostic and therapeutic applications.

Dr. Modolo is the Co-Chair of the Non-Ionizing Radiation (NIR) Task Group of IRPA (International Radiation Protection Association), and a member of the IEEE ICES Sub-Committee three and EWG (Editorial Working Group). He is also a member of the International Advisory Committee for WHO (World Health Organization) for NIR.

MICAELA LIBERTI (Member, IEEE) received the Laurea degree and the Ph.D. degree in electronic engineering from Sapienza, University of Rome, Italy, in 1995 and 2000, respectively. From 2001 to 2002, she was a Postdoctoral Fellow with the Italian Inter-University Center of Electromagnetic Fields and Biosystems. In 2002, she became an Assistant Professor with the Department of Electronic Engineering, University of Rome La Sapienza, Rome, Italy. Since 2008, she has been a member of the Scientific Council of the European Bioelectromagnetic Association. In 2011, she was the General Chair of EBEA2011. She is in COST TD1104: European network for development of electroporation-based technologies and treatments. Her scientific research interests include interaction mechanisms between EM fields and biological systems, dosimetric evaluations at the microscopic level, exposure systems dosimetry, and design.

FRANCESCA APOLLONIO (Member, IEEE) received the Laurea degree (*cum laude*) in electronic engineering and the Doctorate degree from the Sapienza University of Rome, Rome, Italy, in 1994 and 1998, respectively. In 2000, she became an Assistant Professor with the Department of Electronic Engineering, Sapienza University. Since 2011, she has been a member of the National Scientific Commision CNR-URSI, Commission K Electromagnetics in Biology and Medicine. From 2012 to 2015, she served on the Board of Directors of the Bioelectromagnetic Society (BEMS). Her research focuses on the interaction between electromagnetic fields and biological systems using both theoretical and experimental approaches.

MAXIM ZHADOBOV (Senior Member, IEEE) received the Ph.D. and Habilitation á Diriger des Recherches degrees from the Institut d'Electronique et des Technologies du numerique (IETR), University of Rennes 1, Rennes, France, in 2006 and 2016, respectively.

He was a Postdoctoral Researcher with the Center for Biomedical Physics, Temple University, Philadelphia, PA, USA, until 2008, and then joined the French National Center for Scientific Research (CNRS).

He is currently Senior Research Scientist with the IETR/CNRS In Charge of the Electromagnetic Waves in Complex Media (eWAVES) research group. He has coauthored five book chapters, more than 80 research papers in peer-reviewed international journals, and 180 contributions to conferences and workshops. His research interests include innovative biomedical applications of electromagnetic fields and associated technologies. His review article in the *International Journal of Microwave and Wireless Technologies* was the most cited paper in 2016–2020. A paper published by his research group in 2019 is in journal Top 100 of Nature Scientific Reports. He has been involved in 25 research projects (13 as PI).

Dr. Zhadobov was the TPC Co-Chair of BioEM 2021/2020. He was a TPC member and/or session organizer at international conferences, including EUMW2022, IEEE IMBioC 2022, AT-AP-RASC 2022, BioEM 2019, EuMW 2019, IEEE iWEM 2017, MobiHealth 2015–2017, BodyNets 2016, and IMWS-Bio 2014. He is an elected member of EBEA Council, member of IEEE TC95.4, and Vice-President of URSI France Commission K. He is an Associate Editor for IEEE JOURNAL OF ELECTROMAGNETICS, RF AND MICROWAVES IN MEDICINE AND BIOLOGY and was the Guest Editor of several special issues, including Human Exposure in 5G and 6G Scenarios of Applied Sciences and Advanced Electromagnetic Biosensors for Medical, Environmental and Industrial Applications of Sensors. He was also on review boards of more than 15 international journals and conferences, and has been acting as an expert at research councils worldwide. He was the recipient of the CNRS Medal in 2018, the EBEA Award for Excellence in Bioelectromagnetics in 2015, and Brittany's Young Scientist Award in 2010. Since 2010, his Ph.D. students have been recipients of seven national scientific awards and five awards from the Bioelectromagnetics Society, URSI, and IEEE Antennas and Propagation Society.